Comparative analysis of clutter suppression techniques for landmine detection using ground penetrating radar

Ahmet Burak Yoldemir, Rıdvan Gürcan, Gülay Büyükaksoy Kaplan, Mehmet Sezgin
TÜBİTAK BİLGEM, Information Technologies Institute, Gebze, Kocaeli, Turkey

ABSTRACT

In this study, we provide an extensive comparison of different clutter suppression techniques that are proposed to enhance ground penetrating radar (GPR) data. Unlike previous studies, we directly measure and present the effect of these preprocessing algorithms on the detection performance. Basic linear prediction algorithm is selected as the detection scheme and it is applied to real GPR data after applying each of the available clutter suppression techniques. All methods are tested on an extensive data set of different surrogate mines and other objects that are commonly encountered under the ground. Among several algorithms, singular value decomposition based clutter suppression stands out with its superior performance and low computational cost, which makes it practical to use in real-time applications.

Keywords: Ground penetrating radar, clutter suppression, background removal, landmine detection

1. INTRODUCTION

Ground penetrating radar (GPR) is a non-invasive geophysical tool that is used for subsurface imaging.[1] GPR can be used in a wide variety of applications, one of which is the landmine detection problem. Conventionally, metal detectors (electromagnetic induction sensors) were used for landmine detection, however, metal detectors are not capable of finding landmines that include little or no metal content. GPR, on the other hand, can find such objects by detecting differences in the dielectric properties under the inspected area. GPR has several advantages including rapid scanning, good penetration depth, and being able to operate in most environments.[2] However, landmine detection using GPR is a difficult task as the returning signal is generally dominated by the ground reflection, ringing noise and clutter signals. Here, clutter refers to inhomogeneities and cavities inside the ground and buried rubbish. Especially in detection of deeply buried plastic mines, the target signature may be completely masked if the unwanted signals are not properly removed. We use the term clutter suppression for the general problem of removing these unwanted signals. For the removal of such signals, several alternatives were proposed. Some of them ignore the nonstationarity of the clutter and the roughness of the ground surface. In more complex methods, adaptive approaches are adopted to account for these changes. There are some review articles on clutter suppression in literature.[3–5] However, these reviews either deal with too simplistic solutions or they compare too few techniques. Moreover, in these comparisons, the conclusions are drawn based on visual inspection or signal to noise ratio (SNR) values. Hence, the effect of the clutter suppression algorithms on the detection performance is not clear. In this study, we present a comprehensive comparison of available methods, and using a well-known detection algorithm, detection performances are compared. Results are given based on receiver operating characteristic (ROC) curves, which are probability of detection versus probability of false alarm graphs.

Further author information: (Send correspondence to A.B.Y.)
A.B.Y.: E-mail: burak.yoldemir@bte.tubitak.gov.tr
R.G.: E-mail: ridvan.gurcan@bte.tubitak.gov.tr
G.B.K.: E-mail: gulay.kaplan@bte.tubitak.gov.tr
M.S.: E-mail: mehmet.sezgin@bte.tubitak.gov.tr

Detection and Sensing of Mines, Explosive Objects, and Obscured Targets XVI,
edited by Russell S. Harmon, John H. Holloway Jr., J. Thomas Broach, Proc. of SPIE
Vol. 8017, 80171U · © 2011 SPIE · CCC code: 0277-786X/11/$18 · doi: 10.1117/12.895415

2. METHODS

In this section, summary of the techniques compared in this study is given. A convention for data representation is adopted in the presentation of all methods. An A-scan, which is the 1D GPR signal recorded at a specific point is denoted as $A_i(t)$, where $i = 1, 2, \ldots, N$ is the index of the A-scan and $t = 1, 2, \ldots, M$ is the depth index. Merging the A-scans taken at consecutive positions results in a 2D GPR signal of size $M \times N$, which is termed as a B-scan. ith depth bin of the B-scan is denoted as $\mathbf{x}_i$. This representation is a simplistic one which ignores lateral variations in wave velocity. Actually, each sample of $\mathbf{x}_i$ are not necessarily at exactly the same depth.

2.1 Subtraction of the average A-scan

In this method, an ensemble of A-scans taken at a target-free region are averaged, and this average A-scan is used as the background estimate.[1] This method assumes that the clutter distribution does not considerably change with position. This operation can be shown as

$$\overline{A_k}(t) = A_k(t) - \frac{1}{L}\sum_{i=1}^{L} A_i(t) \tag{1}$$

where L is the number of A-scans to be averaged, and $k = 1, 2, \ldots, N$ is the index of the A-scan.

2.2 Subtraction of the median A-scan

This technique is very similar to the previous method. The averaging operation is changed with a median filter. The median filtering is done on a row-by-row basis, i.e., 1D median filtering is performed at each depth bin, with a window size of 5 samples.

2.3 Singular value decomposition

Clutter suppression based on singular value decomposition (SVD) is proposed by many authors.[6–9] All of these papers more or less describe the same method, i.e., using high-pass eigenimages of GPR signals. Using high-pass eigenimages effectively removes the highly correlated parts of the traces. These correlated parts often correspond to the flat reflections in the B-scans.

SVD is a factorization of a rectangular matrix $\mathbf{X}$ of size $M \times N$ into orthogonal matrices as $\mathbf{X} = \mathbf{U}\mathbf{\Sigma}\mathbf{V}^T$, where $\mathbf{U}$ is an $M \times M$ unitary matrix, $\mathbf{\Sigma}$ is an $M \times N$ diagonal matrix, and $\mathbf{V}$ is an $N \times N$ unitary matrix. The singular values of $\mathbf{X}$ are stored in the main diagonal of $\mathbf{\Sigma}$ in decreasing order. Columns of $\mathbf{U}$ are termed as the left singular vectors of $\mathbf{X}$, and those of $\mathbf{V}$ are the right singular vectors of $\mathbf{X}$. Depending on the linear dependence among A-scans, a B-scan can be reconstructed using only some eigenimages. If all A-scans are linearly independent, perfect reconstruction of $\mathbf{X}$ is only possible by using all eigenimages. On the other hand, if all A-scans are linearly dependent, only one eigenimage is enough to reconstruct $\mathbf{X}$. Hence, the number of eigenimages to be used in reconstruction should be selected according to the degree of dependence between A-scans. During our tests, we observed that discarding only the eigenimage with the largest singular value and reconstructing the B-scan using the remaining eigenimages gives satisfactory results.

2.4 Wavelet transform

Wavelet transform is also used to suppress clutter inherent in GPR signals.[10,11] In this method, the data is transformed into the wavelet domain, and wavelet coefficients corresponding to clutter signatures are canceled. After this canceling operation, inverse wavelet transform gives the enhanced GPR data, where clutter is suppressed.

Wavelet transform is very similar to Fourier transform, except that their bases are different. Wavelet transform can provide both time and frequency localization simultaneously. In this method, instead of each A-scan, each depth bin in the B-scan is inspected. Each $\mathbf{x}_i$ is decomposed into L wavelet levels. The wavelet coefficients corresponding to $\mathbf{x}_i$ is denoted by $W_i^j(k)$, where $j = 1, 2, ..., L$ is the decomposition level and $k = 1, 2, ..., K$, where $K = N/2j$.

Clutter is assumed to have a Gaussian distribution and each $W_i^j(k)$ is tested for Gaussianity. Skewness is used as the measure of Gaussianity. For a given $W_i^j(k)$, skewness is denoted as

$$S = \frac{E\left\{\left(W_i^j(k)\right)^3\right\}}{\left\{E\left\{\left(W_i^j(k)\right)^2\right\}\right\}^{1.5}}. \tag{2}$$

As we have a finite number of samples, sample skewness formula is adopted instead of (2). Sample skewness is given by

$$\hat{S} = \frac{1}{K}\sum_{k=1}^{K}\left(\frac{W_i^j(k)-\mu}{\sigma}\right)^3 \tag{3}$$

where $\mu = E\left\{W_i^j\right\}$ and $\sigma^2 = E\left\{\left(W_i^j-\mu\right)^2\right\}$. In the Gaussianity test, an interval for skewness value is allowed, which can be expressed as $-\gamma < \hat{S} < \gamma$.

If the skewness value for a certain decomposition level for a given depth bin falls within this interval, the distribution of the wavelet coefficients at that decomposition level is concluded to have a Gaussian distribution. In this case, the coefficients corresponding to the Gaussian distribution are equated to zero. It is important to note that each decomposition level for a given depth bin is separately tested for Gaussianity, i.e., a certain decomposition level of $\mathbf{x}_i$ might have a Gaussian distribution whereas others do not. During our experiments, 5th order coiflets are found to be working well for our purposes in transforming the raw data to wavelet domain.

2.5 Radon transform

Radon transform for enhancing GPR signals is proposed in Ref. 12, especially for removing ringing noise. There are several variants of Radon transform in literature. This study focuses on the linear Radon transform. In linear Radon transform, straight lines in time-distance $(t-x)$ plane are mapped to points in intercept-slope $(\tau-p)$ domain. The correlated components among A-scans are seen as horizontal lines in B-scans. Hence, these horizontal lines will be mapped to $p=0$ axis after applying linear Radon transform. Hence, $p=0$ axis of the data in the transformed domain can be equated to zero to remove these components. Finally, inverse Radon transform can be applied to obtain the enhanced GPR signal.

2.6 Independent component analysis

The objective of independent component analysis (ICA) is extracting latent independent sources from the observed signals. For this reason, it can be applied to GPR signal in order to remove the background.[13] In ICA, the source signals are assumed to be independent and to have non-Gaussian distributions.[14] ICA aims to find a linear transformation such that the resulting components are independent from each other as much as possible. In the simplest form of ICA, observed variables $\mathbf{x}$ are assumed to be generated by $\mathbf{x} = \mathbf{As}$, where $\mathbf{A}$ is called mixing matrix and $\mathbf{s}$ represents independent components. In ICA, both $\mathbf{A}$ and $\mathbf{s}$ are estimated using $\mathbf{x}$. In other words, the task of ICA is to estimate the mixing matrix $\mathbf{A}$ or its inverse $\mathbf{A^{-1}} = \mathbf{W}$ (demixing matrix) such that elements of the estimate $\mathbf{s} = \mathbf{Wx}$ are as independent as possible. In literature, several methods are available for computing the independent components and the mixing matrix.[14] In this study we utilized the fixed-point ICA algorithm.

In this study we assume that observed signals are linearly composed of two source signals, target and background, similar to Ref. 15 and Ref. 16. Due to the nature of ICA, amplitude and sign of independent components are ambiguous. In order to find the background component, the first A-scan which is assumed to be the representative of the background signal is correlated with four components, i.e., original independent components and their mirrored versions with respect to $y=0$ axis. The component with the highest correlation score corresponds to the background signal. This solves both amplitude and sign ambiguities. The target signal is determined by multiplying the mixing matrix with the independent component corresponding to the target signature. In order to find the mixing matrix and two independent components, FastICA was used.[17] In the experiments, we chose $g(y) = y^3$ as a measure of non-Gaussianity and deflation scheme for estimation process.

2.7 Migration

The B-scan in the time domain suffers from the diffraction hyperbolae of a buried object.[18] Migration techniques can be used to suppress the hyperbolic character of objects' reflections. By considering the velocity of the electromagnetic waves in the soil, migration process creates the target reflector surface from the record surface. After applying migration, the final image has better resolution and improved signal to clutter ratio by collapsing the diffraction hyperbolae. On the other hand, performing the migration with a wrong velocity can result in U shaped target signatures in the output image. Generally, migrated images have reduced relative signal amplitude and this can degrade the detection performance, depending on the detection scheme. In this study, we applied the Stolt migration technique to process the B-scans.

Consider the radar signal $u(x, z, t)$ which satisfies the wave equation

$$\nabla^2 u(x, z, t) - \mu\epsilon \frac{\partial^2}{\partial t^2} u(x, z, t) = 0 \tag{4}$$

where x is the distance along the swinging direction, z is depth, t is time, μ is permeability of the free space and ϵ is permittivity of the free space. Stolt migration solves (4) for $t = 0$ and the generates the migrated image $\hat{u}(x, z)$.

2.8 Backprojection

Standard backprojection technique can also be used to remove the diffraction hyperbolae of a buried object.[19] Similar to migration, standard backprojection algorithm geometrically relocates the object and increases the resolution of the image. Signature of an ideal point-like reflector forms a hyperbolic structure in the space-time domain. For every pixel of the image, backprojection applies coherent summation along the diffraction hyperbolae as if that pixel contains the buried object. For pixels that actually belong to target locations, summations will result in large values, effectively increasing the contrast in the B-scan and collapsing the diffraction hyperbolae. Like migration, finding the wave velocity accurately is crucial for backprojection, as selecting a wrong wave velocity will result in distorted B-scans.

3. DETECTION ALGORITHM

The detection algorithm that is used the to compare the effect of the aforementioned clutter suppression techniques on the detection performance is the basic linear prediction scheme in time domain, frequency domain counterpart of which was introduced in Ref. 20. This method will be briefly explained in this section. For more details, see Ref. 20.

The underlying principle of using linear prediction in detection of buried objects is that, similarity between different clutter signatures is considerably higher than the similarity between clutter signatures and target signatures. Hence, using the clutter signatures that were previously recorded, we can model the new clutter signatures, but we cannot model the target signatures.

Let $\mathbf{X}_i(k) = [A_1(t), A_2(t), ..., A_N(t)]$ represent the ensemble of A-scans, where i is the index in the swinging direction of the detector, t is the depth index and N is the number of gathered A-scans. Let each A-scan be composed of M samples. The linear prediction model for the A-scans can be stated as

$$\hat{A}_i(t) = \sum_{m=1}^{p} a_m A_{i-m}(t) \tag{5}$$

where $\hat{A}_i(t)$ is the predicted A-scan, p is the prediction order and a_m is the mth linear prediction coefficient. For simplicity, we can express the linear prediction model in matrix form as

$$A_i(t) = \sum_{m=1}^{p} a_m A_{i-m}(t) + \varepsilon_i(t) = \overline{\mathbf{X}}_p(t)\mathbf{a}_i(m) + \varepsilon_i(t) \tag{6}$$

where $\varepsilon_i(t)$ is the prediction error vector, $\overline{\mathbf{X}}_p(t)$ is the matrix formed of the most recent p A-scans and $\mathbf{a}_i(m) = [a_1, a_2, ..., a_p]$ is the prediction coefficients vector for the current scanning location. A good fit to linear prediction model implies that energy of the prediction error vector, which is given as

$$\zeta_{\varepsilon_i} = \varepsilon_i(k)^T \varepsilon_i(k) \tag{7}$$

is low. To calculate the linear prediction coefficients, maximum likelihood approach is adopted. We model the elements of the prediction error vector as independent and identically distributed zero-mean Gaussian random variables with variance σ^2. This assumption implies that $A_i(t)$ has an M-variate Gaussian distribution when there is no target in the penetration range. Minimizing the likelihood of this M-variate Gaussian probability density function, we get the following maximum likelihood estimate for $\mathbf{a}_i(m)$:

$$\hat{\mathbf{a}}_i(m) = (\overline{\mathbf{X}}_p(t)^T \overline{\mathbf{X}}_p(t))^{-1} \overline{\mathbf{X}}_p(t)^T A_i(t). \tag{8}$$

ζ_{ε_i} for this maximum likelihood estimate of linear prediction coefficients becomes the test statistic, i.e., the detection function.

4. EXPERIMENTAL RESULTS

In this section, detection results obtained after applying each of the clutter suppression techniques are given. The data set consists of real GPR measurements taken with the hand held landmine detector developed at The Scientific and Technological Research Council of Turkey.[21] Several surrogate landmines and other objects that are commonly encountered under the ground are used in the tests. Table 1 tabulates the target types and number of B-scans measured from each object type.

Table 1. Data set used in the experiments

Object type	**Number of signatures**
TS50 surrogate mine	20
VS50 surrogate mine	20
PMD surrogate mine	20
PMN surrogate mine	20
M15 surrogate mine	20
TM62M surrogate mine	20
M7A2 surrogate mine	20
VS1.6 surrogate mine	20
Rock	20
Glass bottle	20
TOTAL	**200**

Surrogate mines are extremely similar to their corresponding landmines in terms of size and content. The buried rock's longest edge is 8 cm. The glass bottle has a height of 18 cm and the radius of its largest cross section is 4 cm. Burial depth of each object is approximately 10 cm.

ROC curve is a probability of detection (P_d) versus probability of false alarm (P_{FA}) graph, where each point on the curve corresponds to a specific threshold. A detection alarm is given if there are 5 consecutive samples in the inspected area with detection function values greater than the threshold. 5 consecutive samples correspond to a target width of about 2.1 cm. The P_d and P_{FA} definitions are similar to the ones in Ref. 20. P_d is equal

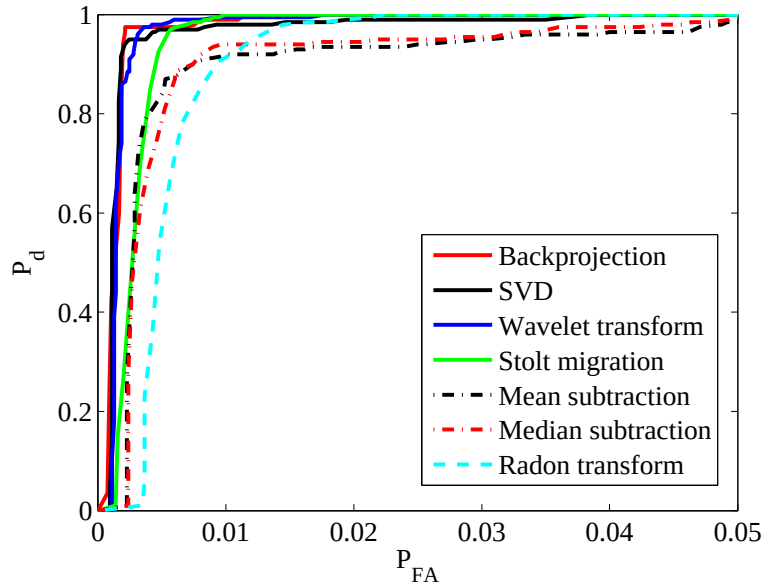

Figure 1. Comparison of ROC curves for each clutter suppression method

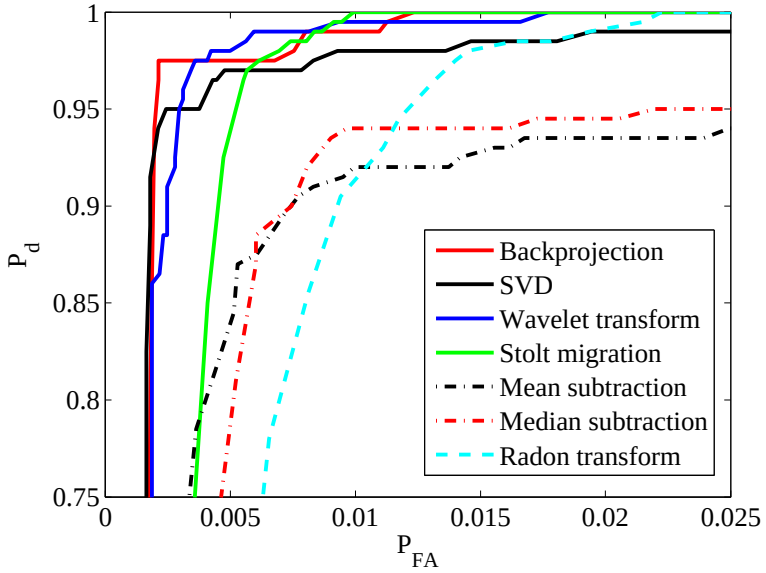

Figure 2. Close up of ROC curves' comparison

to the number of correct alarms divided by the total number of B-scans. P_{FA} is equal to the number of false alarms divided by the number of maximum possible false alarms. For a certain threshold setting, a target is detected if there is an alarm within 8 cm from the edge of the object with detection function value greater than the threshold. The remaining areas are defined to be the false alarm zones. Number of maximum possible false alarms is the ceiling of the number of false alarm positions divided by 5, which is the alarm size corresponding to 2.1 cm. Using these definitions, ROC curves for each of the clutter suppression techniques are given in Fig. 1.

As seen in Fig. 1, detection results of each method are fairly comparable. Detection result after applying ICA based clutter suppression was much worse than each of these techniques, and is not given here. Using ICA technique, a P_{FA} value of 0.13 was obtained for a P_d value of 0.95. To better analyze the results, a close-up of Fig. 1 is given in Fig. 2.

In ROC curve analysis, the aim is to reach to the top left part of the plot as much as possible, which is

the perfect detection point with no false alarms. As seen from Fig. 2, backprojection method provides the best performance compared to other methods for a P_d value of 0.95. However, computational cost of backprojection is highest among all considered techniques. This cost makes backprojection implausible in real-time applications. SVD and wavelet transform based techniques give fairly comparable results to backprojection. Particularly, SVD based clutter suppression is a very light-weight technique which will work in real-time applications without any problems. After these methods, Stolt migration achieved the best performance for P_d=0.95. Conventional mean and median subtraction techniques and Radon transform gave similar results and they are the worst performing techniques compared to others.

If the system is meant to work in real-time, we conclude that SVD based clutter suppression technique is optimal. If offline processing of data is viable, backprojection technique should be selected. Computational cost of wavelet transform technique is between these two, however, it requires to set a threshold to the allowed skewness value. Selection of this threshold may change according to system specifications and soil type. Hence, this method should be avoided to come up with a global algorithm which can be used to scan any type of ground in conjunction with any detector hardware.

It should be emphasized that, the data set used in this study was gathered on a controlled terrain. On an uncontrolled terrain, false alarm rates are expected to increase. Moreover, one cannot confidently state that SVD based clutter suppression will work better than any other technique in detection of buried targets. This study only reflects the performances of these preprocessing algorithms combined with the linear prediction based detection algorithm.

5. CONCLUSION

This paper presented a comprehensive comparative analysis of the effect of different clutter suppression techniques on the buried object detection performance. Among several algorithms, clutter suppression techniques based on SVD, backprojection, wavelet transform and Stolt migration are shown to outperform others. Specifically, SVD based preprocessing technique is shown to be the optimal technique when computational cost is also considered. Results are presented on ROC curves. Combination of SVD based preprocessing and linear prediction based detection algorithm provided a false alarm rate of less than 0.3% at a detection rate of 95% on a controlled terrain.

REFERENCES

[1] Daniels, D. J., [*Ground Penetrating Radar*], The Institution of Electrical Engineers, London, UK, second ed. (2004).

[2] Witten, T. R., "Present state-of-the-art in ground penetrating radars for mine detection," *Proc. SPIE 3392* (1998).

[3] Abujarad, F., Jostingmeier, A., and Omar, A. S., "Clutter removal for landmine using different signal processing techniques," *Proc. 10th IEEE International Conference on Ground Penetrating Radar* (2004).

[4] Mayordomo, A. M. and Yarovoy, A., "Optimal background subtraction in GPR for humanitarian demining," *Proc. 5th European Radar Conference* (2008).

[5] Tjora, S., Eide, E., and Lundheim, L., "Evaluation of methods for ground bounce removal in GPR utility mapping," *Proc. 10th IEEE International Conference on Ground Penetrating Radar* (2004).

[6] Cagnoli, B. and Ulrych, T. J., "Singular value decomposition and wavy reflections in ground-penetrating radar images of base surge deposits," *J. Appl. Geophys.* **48**, 175–182 (2001).

[7] Khan, U. S. and Al-Nuaimy, W., "Background removal from GPR data using eigenvalues," *Proc. 13th IEEE International Conference on Ground Penetrating Radar* (2010).

[8] Shaw, A. K. and Bhatnagar, V., "Automatic target recognition using eigen-templates," *Proc. SPIE 3370* (1998).

[9] Gunatilaka, A. and Baertlein, B. A., "A subspace decomposition technique to improve GPR imaging of anti-personnel mines," *Proc. SPIE 4038* (2000).

[10] Yoldemir, A. B. and Sezgin, M., "Depth estimation of buried objects using wavelet transform and statistical hypothesis testing," *Proc. SPIE 7664* (2010).

[11] Abujarad, F., Nadim, G., and Omar, A., "Wavelet packets for GPR detection of non-metallic anti-personnel land mines based on higher-order-statistic," *Proc. 3rd International Workshop on Advanced Ground Penetrating Radar* (2005).

[12] Kim, J.-H., Cho, S.-J., and Yi, M.-J., "Removal of ringing noise in GPR data by signal processing," *Geosciences Journal* **11**, 75–81 (2007).

[13] Morgenstjerne, A., Karlsen, B., Larsen, J., Sørensen, H., and Jakobsen, K., "A comparative and combined study of EMIS and GPR detectors by the use of independent component analysis," *Proc. SPIE 5794* (2005).

[14] Hyvarinen, A., Karhunen, J., and Oja, E., [*Independent Component Analysis*], John Wiley & Sons, Inc., NY, USA (2001).

[15] Verma, P. K., Gaikwad, A. N., Singh, D., and Nigam, M. J., "Analysis of clutter reduction techniques for through wall imaging in UWB range," *Progress In Electromagnetics Research B* **17**, 29–48 (2009).

[16] Karlsen, B., Larsen, J., Sørensen, H., and Jakobsen, K., "Comparison of PCA and ICA based clutter reduction in GPR systems for anti-personnel landmine detection," *Proc. 11th IEEE Workshop on Statistical Signal Processing* (2001).

[17] Hyvarinen, A., "Fast and robust fixed-point algorithms for independent component analysis," *IEEE Trans. Neural Networks* **10**, 626–634 (1999).

[18] Kabourek, V. and Cerny, P., "SAR and Stolt migration processing for plastic landmine detection," *Proc. 20th International Conference Radioelektronika* (2010).

[19] Gurbuz, A. C., McClellan, J. H., and Scott, W. R., "Imaging of subsurface targets using a 3D quadtree algorithm," *Proc. IEEE International Conference on Acoustics, Speech, and Signal Processing* (2005).

[20] Ho, K. C. and Gader, P. D., "A linear prediction land mine detection algorithm for hand held ground penetrating radar," *IEEE Trans. Geosci. Remote Sensing* **40**(6), 1374–1384 (2002).

[21] Sezgin, M., "Development of dual sensor hand-held detector," *Proc. SPIE 7664* (2010).